Journal of Molecular Structure 1217 (2020) 128430

Contents lists available at ScienceDirect

Journal of Molecular Structure

journal homepage: http://www.elsevier.com/locate/molstruc

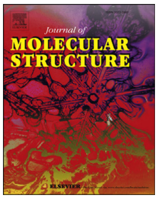

Systematic study of the fluorescent properties of cinnamaldehyde phenylhydrazone and its interactions with metals: Synthesis and photophysical evaluation

Marco Mellado [a], [*], Rafaela Sariego-Kluge [a], César González [b], Katy Díaz [b], Luis F. Aguilar [a], Manuel A. Bravo [a], [**]

[a] Instituto de Química, Facultad de Ciencias, Pontificia Universidad Católica de Valparaíso. Av. Universidad #330, Curauma, Valparaíso, Chile
[b] Departamento de Química, Universidad Técnica Federico Santa María. Av. España 1680, Valparaíso, Chile

ARTICLE INFO

Article history:
Received 21 March 2020
Received in revised form
8 May 2020
Accepted 9 May 2020
Available online 11 May 2020

Keywords:
Cinnamaldehyde phenylhydrazone
Selective fluorescence quenching
Thermodynamic properties
HOMO -LUMO electron transfer

ABSTRACT

Hydrazones are organic compounds with applications in various fields of research, including fluorescent applications. In this investigation, the compound cinnamaldehyde phenylhydrazone was synthesized by condensation between cinnamaldehyde (**1**) and phenylhydrazine (**2**). Furthermore, the photophysical properties were evaluated in the presence and absence of inorganic salts, and it was found that the fluorescence intensity selectively decays with $CuCl_2$ in a thermodynamically spontaneous process (ΔG = negative). In addition, computational approaches were used, which identified the transfer of electrons from highest-occupied molecular orbital HOMO of compound **3** to the lowest unoccupied molecular orbital (LUMO) of $CuCl_2$ as the key interaction for quenching the fluorescence intensity of cinnamaldehyde phenylhydrazone.

Additionally, the potential application of compound **3** as a Cu^{2+} chemosensor in different water samples was evaluated. This compound was found to exhibit better recovery of Cu^{2+} in natural water samples (higher than 99.3%) than in drinking water (66%).

1. Introduction

Hydrazones are known as Schiff bases that can be obtained by condensation between hydrazines and aldehydes, exhibiting an N=C bond [1]. These compounds have important properties for use in various fields of research (*e.g.*, pharmacology). Hydrazones are used as “building blocks” for the development of bioactive molecules (showing analgesic, anti-inflammatory, antioxidant, antidepressant, anti-convulsant, anti-acetylcholinesterase, antitumour, anti-tuberculosis, and broad-spectrum antimicrobial activities) [2–18]. Additionally, hydrazones have fluorescent properties, so they can be used as pigments, dyes, molecular switches, metallo-assemblies, and sensors [19–23]. Regarding its use as a sensor, hydrazone can coordinate with various transition metals to form stable complexes, including Cu(II), Fe(III), and Zn(II) [24–27].

The development of organic molecules with colorimetric or fluorescent chemosensor properties to detect toxic metal ions, *e.g.*, Cu^{2+}, has received great attention [28]. This cation plays several roles in living systems, among which it functions as a nutrient and redox catalyst in metalloenzymes such as carbonic anhydrase, carboxypeptidases, alkaline phosphatase and β-lactamase [29,30]. Despite the important physiological functions of this cation, variations in its concentration in the human body are associated with Alzheimer’s, Wilson and prion diseases, as well as lateral amyotrophic sclerosis and others; all these diseases are related to the production of reactive oxygen species (ROS) [30]. Due to the above mentioned reasons, the determination of trace amounts of copper in drinking water is becoming increasingly important. To this end, compounds with simple chemical structures have been used as colorimetric probes to detect Cu^{2+}such as compound (**I**) [31], while compounds (**II**) and (**III**) have also been used to detect Cu^{2+} but as fluorescent probes (see Fig. 1) [28,32].

To evaluate its possible application as a chemosensor, cinnamaldehyde phenylhydrazone (**3**) was synthesized by condensation between cinnamaldehyde (**1**) and phenylhydrazine (**2**) (see Scheme

---

[*] Corresponding author.
[**] Corresponding author.
E-mail addresses: marco.mellado@pucv.cl (M. Mellado), manuel.bravo@pucv.cl (M.A. Bravo).

https://doi.org/10.1016/j.molstruc.2020.128430

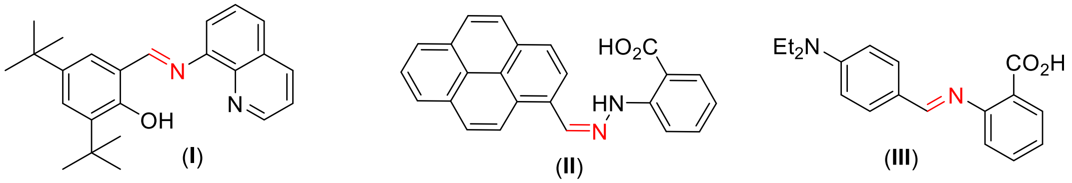

Fig. 1. Hydrazones used to detect and measure Cu(II), with the Schiff base bond highlighted in red.

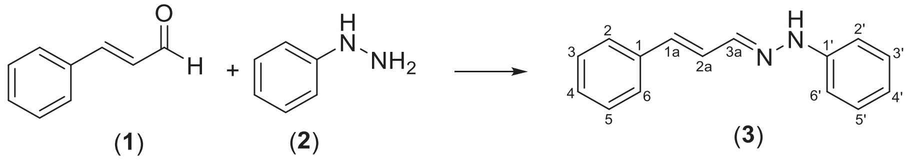

Scheme 1. Synthesis of cinnamaldehyde phenylhydrazone (**3**).

1). Its photophysical properties (UV—Vis and fluorescence) were evaluated in the absence and presence of inorganic (metal) salts, as well as the determination of thermodynamic constants associated with the inorganic metal-hydrazone interaction (ΔG, ΔH, and ΔS). Additionally, the main chemical properties that influence the metal-hydrazone interaction were identified by density functional theory (DFT) calculations and with the application of multivariable analysis. Finally, the potential application of cinnamaldehyde phenylhydrazone (**3**) in the determination of Cu^{2+} in water samples was evaluated.

2. Experimental

2.1. Instrumentation

The melting point was measured using a Stuart Scientific Melting Point SMP3 (Staffordshire, UK). Infrared spectra were recorded using aJasco FT-IR 4600 (Tokyo, Japan). ^{1}H NMR (400.13 MHz), ^{13}C NMR (100.6 MHz), 2D-HSQC and 2D-HMBC spectra were recorded on a Bruker Avance 400 Digital NMR spectrometer (Berlin, Germany). Tetramethylsilane was used as an internal standard. GC-MS was carried out using an Agilent Technologies 6890 model (Santa Clara, CA, USA) with an automatic ALS and an HP MD 5973 mass detector in splitless mode. Measurement of pH was performed using a Bante Instruments Benchtop PHS-25cw microprocessor pH/mV meter (Shanghai, China). Absorption spectra were recorded on a Shimadzu UV-mini-1240 UV—Vis spectrophotometer (Kyoto, Japan). All steady-state fluorescence measurements were performed on an ISS K2 Multifrequency Phase Fluorometer (Champaign, IL, USA).

2.2. Chemicals

Cinnamaldehyde (**1**), phenylhydrazine (**2**), dimethylsulfoxide (DMSO), heptane (C_7H_{16}), tetrahydrofuran (THF), acetone (Me_2CO), dimethylformamide (DMF), methanol (MeOH), HEPES sodium salt HCl, NaOH, LiCl, NaCl, $MgCl_2$ x $6H_2O$, $CaCl_2$ x $2H_2O$, $SrCl_2$ x $6H_2O$, $BaCl_2$ x $2H_2O$, $AlCl_3$, $SnCl_2$ x $2H_2O$, $BiCl_3$, $CrCl_3$ x $6H_2O$, $MnCl_2$ x $4H_2O$, $FeCl_3$ x $6H_2O$, $CoCl_2$ x $6H_2O$, $NiCl_2$ x $6H_2O$, $CuCl_2$ x $2H_2O$, CuCl, $ZnCl_2$, $CdCl_2$ x 2 1/2H_2O, $HgCl_2$, $Pb(NO_3)_2$, $AgNO_3$ and ethylenediamine tetrasodic salt (EDTA), were purchased from Merck (Darmstadt, Germany). 2-Propanol, hexane, dichloromethane (CH_2Cl_2), ethyl acetate and acetonitrile (MeCN) were purchased from J.T. Baker (Radnor, PA, USA).

2.3. Synthesis of cinnamaldehyde phenylhydrazone (3)

In a 250-mL three-neck round-bottomed flask, cinnamaldehyde (**1**, 500 mg, 3.79 mmol) was dissolved in 2-propanol (50 mL), and phenylhydrazine (**2**, 409 mg, 3.79 mmol) was added. The mixture was stirred at reflux for 8 h. After this time, distilled water was added to finish the reaction. The reaction mixture was extracted with dichloromethane (3 × 30 mL), and the organic layer was dried and concentrated under reduced pressure. The resulting mixture was separated using a flash chromatography column with a hexane:ethyl acetate mixture with increasing polarity as the mobile phase. Finally, a pale yellow solid (**3**, 676 mg, 3.07 mmol) was obtained as a pure compound (81% yield); MP: 161.6 ± 1 °C, IR (υ, cm^{-1}): 3441 (s, =N—H), 3313 (s, C=H), 1601 (s, CH Ar), 1560 (m, CH Ar), 1517 (s, CH Ar), 1486 (w, CH Ar), 1259 (s, H—C—N), 1135(s, H—C—N); ^{1}H NMR (400 MHz, $CDCl_3$): δ 7.55 (1H, d, $J = 8.0$ Hz, H-3a), 7.45 (2H, d, $J = 8.0$ Hz, H-2 + H-6), 7.35 (2H, m, H-3'+H-5′), 7.29—7.24 (3H, m, H-3 + H-5 + H-2a),7.06—6.99 (3H, m, H-4+ H-2'+H-6′), 6.87 (1H, m, H-4′), 6.69 (1H, d, $J = 16.0$ Hz, H-1a); ^{13}C NMR (400 MHz, $CDCl_3$): δ 144.2 (C-1′), 139.8 (CH-1a), 136.7 (C-1), 134.1 (CH-3a), 129.3 (2xCH, CH-5' + CH-3′), 128.7 (2xCH, CH-3 + CH-5), 128.0 (CH-4), 126.5 (2xCH, CH-2 + CH-6), 125.9 (CH-2a), 120.2 (CH-4′), 112.7 (2xCH, CH-2' + CH-6'). MS-EI: 222 [M$^+$] (100%). All spectroscopic analyses are consistent with a previous report [1].

2.4. Evaluation of fluorescence spectroscopy parameters

Fluorescence excitation and emission spectra were obtained using a xenon arc lamp as a light source. Fluorescence spectra were measured at 90° in an L-format using single photon counting mode. Data were acquired and analysed by Vinci™ software.

The relative quantum yield (Φ) was determined using quinine-sulfate as a standard (0.1 M H_2SO_4 at 22 °C, $\Phi s = 0.58$, $\lambda_{ex} = 350$ nm) [33]. Equation (1) was used to calculate the quantum yield [34].

$$\Phi = \frac{F_u}{F_s} x \frac{A_s}{A_u} x \frac{n_u^2}{n_s^2} x \Phi_s \qquad \text{(Eq. 1)}$$

where the subscripts u and s indicate the test and standard, respectively. Φ is the quantum yield, A is the absorbance at the excitation wavelength, F is the integrated emission spectrum, and n is the refractive index of the solvent.

2.5. Evaluation of figures of merit

The values of the limit of detection and limit of quantification

(LOD and LOQ, respectively) were calculated as reported by Thompson et al., 2002 using the following equations [35].

$$\mathrm{LOD} = 3*\mathrm{SD}/\mathrm{m} \qquad \text{(Eq. 2)}$$

$$\mathrm{LOQ} = 10*\mathrm{SD}/\mathrm{m} \qquad \text{(Eq. 3)}$$

where SD is the standard deviation of ten blank reagent samples and m is the slope of the calibration curve.

2.6. Computational details

Compound **3**, proposed complex **3-CuCl$_2$**, and all inorganic compounds tested (salts) were optimized using the Gaussian 09 program [36]. To obtain the different chemical properties, a DFT-B3LYP-LanL2DZ optimization was performed. In addition, all optimized geometries were checked by frequency calculations (without any imaginary frequencies) in their potential energy surface.

In addition, quantum reactivity descriptors such as the dipole moment (DM), highest occupied molecular orbital (HOMO), and lowest unoccupied molecular orbital (LUMO) were obtained from the output file, while the chemical potential (μ), hardness (η), softness (S), and global electrophilic index (ω) were calculated with the following equations.

$$\mu = \frac{(E_{LUMO} + E_{HOMO})}{2} \qquad \text{(Eq. 4)}$$

$$\eta = \frac{(E_{LUMO} - E_{HOMO})}{2} \qquad \text{(Eq. 5)}$$

$$S = \frac{1}{2\eta} \qquad \text{(Eq. 6)}$$

$$\omega = \frac{\mu^2}{2\eta} \qquad \text{(Eq. 7)}$$

2.7. Quantitative structure-property relationship (QSPr)

To determine which chemical properties of the different inorganic compounds (salts) produce changes in the fluorescent properties, the quantitative structure-property relationship (QSPr) technique was used through a multiple linear regression similar to that of previous reports of our research group [37,38]. As a dependent variable, the normalized fluorescence intensity (F/F$_0$) of compound (**3**) was used, while as independent variables, the previously mentioned descriptors were used in their linear and quadratic forms (MS, MS^2, MV, MV^2, MW, MW^2, MD, MD^2, DM, DM^2, HOMO, HOMO^2, LUMO, LUMO^2, μ, μ^2, η, η^2, S, S^2, ω, and ω^2) using Statistica 7.0 software.

To ensure that the established relationship is not accidental, the cross-validation technique described by Golbraikh was used according to the following equation [39].

$$q^2 = 1 - \frac{\sum (x_{obs} - \widehat{x})^2}{\sum (x_{obs} - \overline{x})^2} \qquad \text{(Eq. 8)}$$

where x_{obs} is the experimental normalized fluorescence value, $\widehat{x}$ is the calculated normalized fluorescence value and $\overline{x}$ is the average normalized fluorescence value of all compounds. A value equal to or greater than 0.5 is considered acceptable.

2.8. Collection and preparation of water samples

The different water samples corresponding to the different wells were collected in Casablanca Valley (Carpintero's and Pitama's wells), while the drinking water was acquired from Curauma, Valparaíso, Chile. The water samples were filtered using a Millipore Millex HV Hydrophilic PVDF 0.45 μm filter and then subjected to a UCT Cleau-UP® CUC18156 cartridge. Finally, different CuCl$_2$x2H$_2$O solutions were prepared using the different water samples (14, 28, 44, and 72 μM).

3. Results and discussion

3.1. Chemical

When mixing cinnamaldehyde (**1**) with phenylhydrazine (**2**), a few minutes later, a yellow solid appears, corresponding to cinnamaldehyde phenylhydrazone, by nucleophilic attack by the $-NH_2$ group of phenylhydrazine towards the carbonyl carbon of cinnamaldehyde as a classic 1,2-addition reaction to the carbonyl group. After separation of compound **3** from the reaction mixture by column chromatography, the desired compound was confirmed by ^{1}H NMR spectroscopy, showing two doublet signals (δ = 7.27 and δ = 6.69 ppm) with a coupling constant J = 16 Hz, characteristic of a double bond with *trans* geometry. The final structure was determined by complementary NMR experiments (^{13}C, 2D-HSQC and 2D-HMBC) and IR spectroscopy (see **Supplementary Material**), as well as by comparing previous research [1].

3.2. Photophysical measures

Initially, a stock solution of compound **3** was prepared at a concentration of 1.0×10^{-2} M in DMSO, from which a series of dilutions were prepared for the measurement of the different photophysical properties. For the measurement of these properties in the absence of inorganic salts, dilutions were made using MeCN. Additionally, the different inorganic salts were dissolved in deionized water at a concentration of 1.0×10^{-2} M.

For the photophysical measurements associated with molecular absorption, UV–Vis spectra of compound **3** at several concentrations (20, 40, 60, 80 and 100 μM) were recorded using MeCN as the solvent. The UV–Vis spectra showed a maximum absorption at λ_{abs} = 359 nm. The molar extinction coefficient was calculated using the Lambert-Beer law and linear regression ($\varepsilon = 2928.9$ mol^{-1} * cm^{-1} *L, see Supplementary Material Figure S1). Subsequently, the behaviour of the UV–Vis spectrum of compound **3** in the presence of different inorganic salts was evaluated (see Fig. 2). In the presence of CuCl$_2$, a new absorption band is observed to be generated (λ_{abs} = 459 nm), which is attributed to the donation of pairs of non-bonding electrons from nitrogen to the metal [40–42] together with a hypochromic effect on the maximum absorption of compound **3** (λ_{abs} = 359 nm). In contrast, the **3** + CuCl interaction has only a hypochromic effect at λ_{abs} = 359 nm.

Bearing in mind the multiple fluorescent applications that have been reported for hydrazones and to evaluate their application as fluorescent chemosensors, compound **3** was subjected to various tests to evaluate its photophysical properties [20]. The emission and excitation spectra were recorded for compound **3** (0–100 μM). The emission spectrum shows that compound **3** exhibits its maximum fluorescence intensity at λ_{em} = 476 nm when excited at λ_{ex} = 394 nm. The calculated Stokes shift was 82 nm, similar to that of other hydrazones with a more complex structure [31,43]. From the previously described results, the relative quantum yield of compound **3** was calculated using quinine sulfate (ϕ = 0.58) as a standard [33,34], obtaining a value of ϕ = 0.018, similar to that

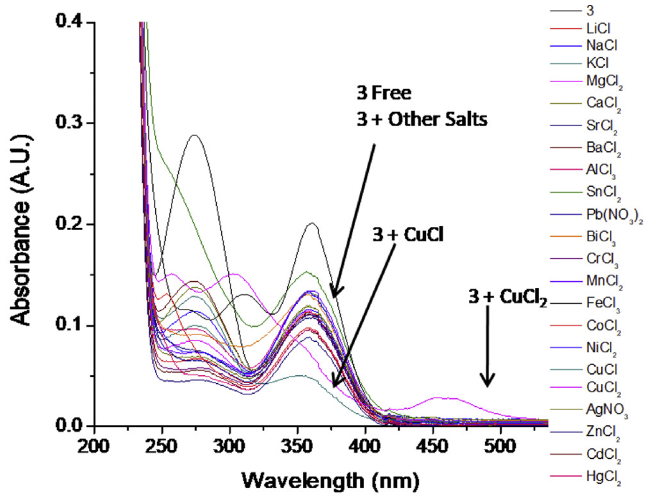

Fig. 2. UV−Vis spectrum of compound **3** (20 μM) and its interaction with different metals (10 molar equivalents).

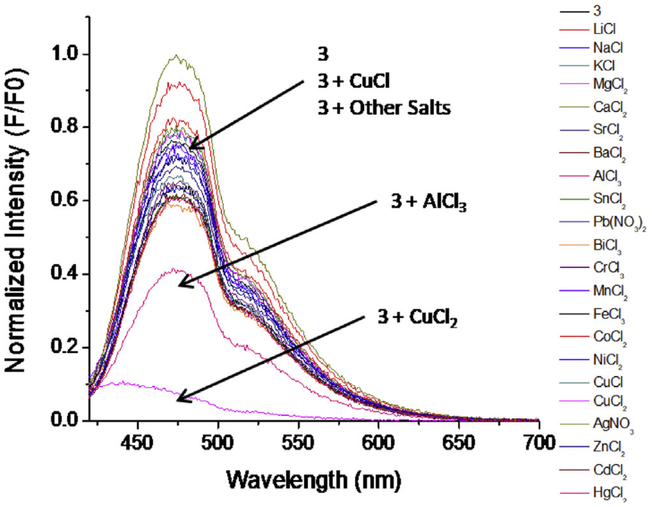

Fig. 3. Emission spectrum of compound **3** and its interaction with different inorganic salts (10 eq. mol). C_3 = 20 μM, solvent = MeCN. λ_{ex} = 394 nm.

reported for a small hydrazone-pyrene-based compound (Supplementary Material Figure S2) [32].

The effect of solvent polarity and pH on the emission spectrum was evaluated. We found that the highest emission intensity was recorded using aprotic polar solvents. On the other hand, it is observed that the emission spectrum has a shift at longer wavelengths when increasing the solvent polarity, consistent with solvent effects shifting the emission to still lower energy due to stabilization of the excited state by the polar solvent molecules [33]. In fact, the best emission was recorded using CH_2Cl_2 (intensity 15177 FUA, see Supplementary Material Figure S3); however, the incompatibility of this solvent with water makes the interaction with inorganic salts unfeasible. Other solvents with high emission were THF, followed by DMF, MeCN, $COMe_2$ and DMSO. It is noted that the emission spectrum of compound **3** using MeCN as a solvent decreases the standard deviation of the measurement (see Supplementary Material Figure S3). The influence of the water content on the emission intensity of compound **3** was investigated, finding that the intensity of the emission decreases proportionally as the percentage of water increases, *e.g.,* when using a 9:1 MeCN:water solution, the fluorescence intensity decreases by 25.4%, while when using only water, the fluorescence intensity decreases by 94.4%. To evaluate the effect of pH on the emission intensity of compound **3**, a series of HEPES buffer solutions at different pH values were used. The results show that the maximum emission intensity is obtained between pH values of 5.0 and 7.0 (see Supplementary Material Figure S3)**.**

Because compound **3** showed an effect on its absorption spectrum when interacting with $CuCl_2$ (see Fig. 1) and because it has fluorescent properties, the effect of copper salts on the emission spectrum of the compound was checked. First, the minimum time required to show significant changes and stability in the interaction of **3**+CuCl and **3**+$CuCl_2$ was determined. The results show that $CuCl_2$ generates a 90% decay of the fluorescence intensity of compound **3** at 3 min of incubation, while CuCl causes a 45% decay of the fluorescence intensity of compound **3** at 15 min (see Material Supplementary Figure S4). Later, the effect of inorganic salts on the emission spectrum of compound **3** was evaluated (see Fig. 3).

Fig. 3 shows that compound **3** does not show a significant variation in fluorescence intensity with all compounds, except $CuCl_2$, which generates a 90% decay of the fluorescence intensity. This effect is due to the intrinsic fluorescence-quenching property that stems from the paramagnetic nature of Cu^{2+} [44]. In addition, when compound **3** interacts with Al^{3+}, it shows a decrease in the fluorescence intensity, corresponding to 60% (30% lower decay than that with $CuCl_2$), which is consistent with that of other phenylhydrazones [28,45]. In cases where fluorescence decay occurs ($CuCl_2$ and $AlCl_3$), it may be associated with the interaction of the hydrazone fragment with the metal centres of the inorganic salts. Contrasting this information with the UV−visible spectra (see Fig. 2), the quenching fluorescence induced by $CuCl_2$ could be related to coordinated bond formation, while $AlCl_3$ quenching fluorescence could be related to the collisional effect because there is no charge-transfer peak.

Subsequently, the quantum yield (ϕ) of compound **3** was evaluated after interacting with $CuCl_2$ and $AlCl_3$ (see Supplementary Material Figure S5). The compound **3**+$CuCl_2$ interaction shows a decay of 55% (ϕ = 0.010) due to the sharp decrease in the absorption and emission bands (see Figs. 3 and 4). However, for the interaction of compound **3**+$AlCl_3$, the quantum yield obtained was ϕ = 0.017 (5.6% lower than that with compound **3**), which is attributed only to a change in the emission spectrum occurring, with the absorption spectrum varying very minimally (see Figs. 1

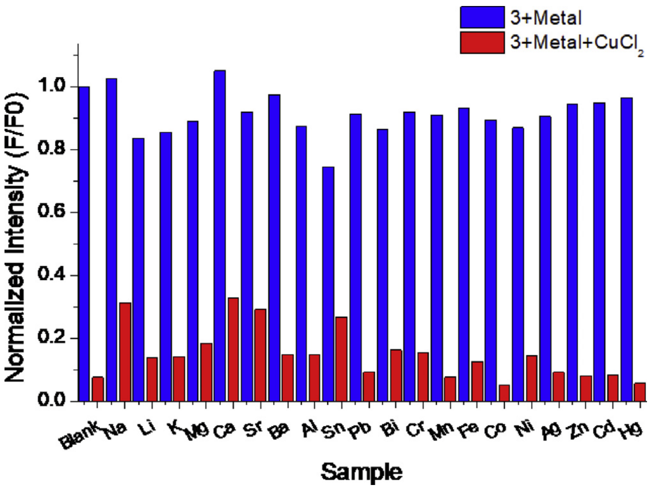

Fig. 4. Selective quenching of the fluorescence intensity of compound **3**. C_3 = 20 μM, C_{salt} = 1.0 eq. mol, solvent = MeCN, λ_{ex} = 394 nm, λ_{em} = 476 nm, $t_{incubation}$ = 3 min.

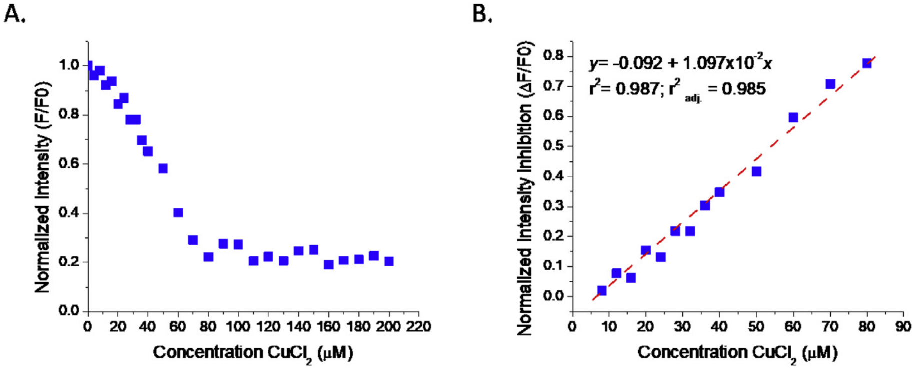

Fig. 5. A. Titration of compound **3** with $CuCl_2$. **B**. Calibration curve used for figures of merit evaluation. $C_3 = 20$ μM, solvent = MeCN, $\lambda_{ex} = 394$ nm, $\lambda_{em} = 476$ nm, T° = 298 K, $t_{incubation} = 3$ min, n = 3.

and 2). This last point is consistent with that mentioned above, and $AlCl_3$ quenching fluorescence could be related to the collisional effect.

To confirm the selective interaction of compound **3** with $CuCl_2$ shown in the previous experiments, we investigated the change in fluorescence intensity in the presence of another inorganic salt and the subsequent addition of $CuCl_2$ (see Fig. 4). Fig. 4 shows that compound **3** in the absence (blank) and presence of all inorganic salts does not change its fluorescence intensity ($F/F_0 \geq 0.8$), except with $SnCl_2$ ($F/F_0 = 0.745$); however, adding $CuCl_2$ generates a significant decrease in the fluorescence intensity ($F/F_0 = \leq 0.2$), except with NaCl, $CaCl_2$, $SrCl_2$ and $SnCl_2$.

To obtain the performance characteristics while monitoring the interaction of Cu^{+2} with compound **3**, a titration was performed at 25 °C using a 20 μM solution of compound **3** in MeCN and adding increasing amounts of $CuCl_2$ in aqueous solution (see Fig. 5A).

Fig. 5A shows the decrease in the fluorescence intensity of compound **3** proportionally to the increase in the $CuCl_2$ concentration. The fluorescence intensity decreased by 80% at 80 μM $CuCl_2$. The detection and quantification limits were calculated from the linear segment of the titration (see Fig. 5B), obtaining LOD = 0.065 μM (8.74×10^{-3} mg/L $CuCl_2$), while the quantification limit was 0.217 μM (2.91×10^{-2} mg/L $CuCl_2$). These results indicate that compound **3** could be used to monitor $CuCl_2$ concentrations in water samples since the detection of this metal is of interest for both biological and environmental sciences [46]. In this sense, the maximum copper allowed is 1.3 mg/L (20 μM) in drinking water according to the U.S. Environmental Protection Agency (EPA) [47]. The results show that compound **3** interacts selectively with $CuCl_2$, whereby the stoichiometry of this interaction was determined. Stoichiometry was determined by the Job plot, showing that the ratio is 1:1 (see Fig. 6A). In addition, the association constant (K) between compound **3** and $CuCl_2$ was calculated by the Benesi-Hildebrand (BH) expression [48] using linear regression between $(F_0{-}F)^{-1}$ and $1/Cu^{2+}$ ($r^2 = 0.963$), where $K_{BH} = 1.22 \times 10^{-2}$ M^{-1} was obtained (see Fig. 6B).

As shown above, the fluorescence intensity of compound **3** decreases by its interaction with $CuCl_2$, so the quenching constant was determined by means of the Stern-Volmer equation (Eq. (9))

$$F_0 \,/\, F = 1 + K_{SV}[Q] \qquad \text{(Eq. 9)}$$

Here, F_0 and F are the fluorescence intensities in the absence and presence of the quencher, respectively, K_{SV} is the dynamic quenching constant and $[Q]$ is the concentration of the quencher.

Various processes can cause fluorescence quenching. The most common processes are complex formation (static quenching) and collisional quenching (dynamic quenching) [49]. One of the ways to distinguish between the phenomena is temperature dependence. If K_{SV} decreases with increasing temperature, it could be considered a static quenching process [50]. Therefore, the variation in the Stern-Volmer constant was measured at 298 K and 308 K (see Fig. 7).

The results for the interaction between compound **3** and $CuCl_2$ indicate a decrease in the Stern-Volmer constant from 1.70×10^4 to 298 K to 1.07×10^4 to 308 K (see Fig. 7), showing that there is a high probability that the quenching phenomenon originates from the

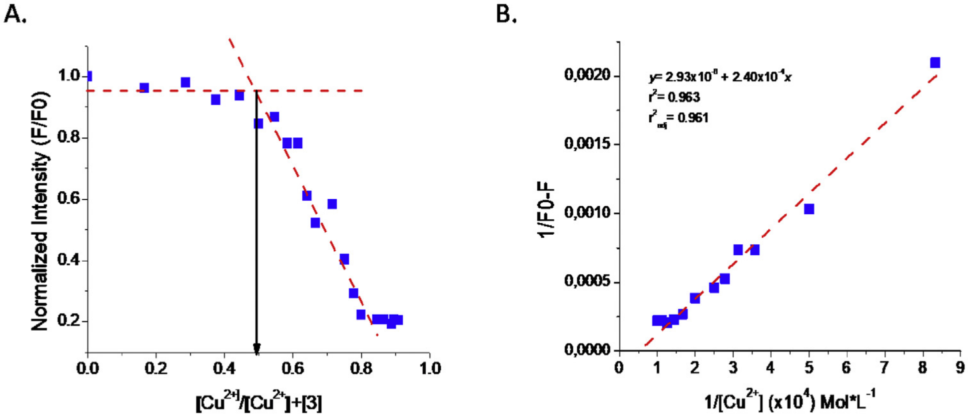

Fig. 6. A. Job plot for the compound **3-$CuCl_2$** interaction. **B.** Benesi-Hildebrand plot based on the 1:1 stoichiometry of the compound **3-$CuCl_2$** interaction. $C_3 = 20$ μM, solvent = MeCN, $\lambda_{ex} = 394$ nm, $\lambda_{em} = 476$ nm, T° = 298 K, $t_{incubation} = 3$ min, n = 3.

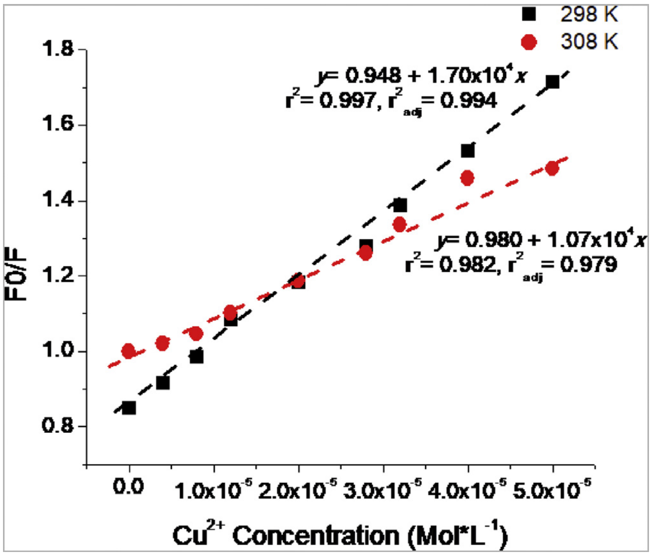

Fig. 7. Determination of Stern-Volmer quenching constants (K_{SV}) for the interaction between compound **3** and $CuCl_2$ at 298 K and 300 K.

formation of a complex [50]. These results agree with the $CuCl_2 \rightarrow$ **3** charge transfer signal shown in Fig. 1 ($\lambda_{abs} = 459$ nm) due to the donation of the non-bonding electron pairs of nitrogen to the metal [40–42], forming a complex. Using the static quenching model, from the intensity-quencher concentration relationship, the binding constant was calculated according to the following equation [49]:

$$log\left[\frac{F_0 - F}{F}\right] = logK + nlog[Q] \tag{Eq. 10}$$

Here, K is the binding constant and n is the number of binding sites per compound **3**. The binding results showed logK = 8.797 at 298 K, while at 308 K, logK = 5.119. In addition, the linear correlation coefficients for both temperatures were larger than 0.99. From these values, as well as the van't Hoff equations, the thermodynamic parameters ΔG, ΔH, and ΔS were determined, according to a previous report [49]. The results of the thermodynamic parameters of the interaction of compound **3** and $CuCl_2$ are shown in Table 1.

The negative value of the Gibbs free energy change (ΔG) indicates that the interaction between compound **3** and $CuCl_2$ is a spontaneous process. The positive value of ΔS is characteristic of chelation processes, where the solvent molecules are arranged around compound **3** and the interaction of $CuCl_2$ causes the disorder of these molecules and anincrease in the configurational entropy [51]. The positive value of the enthalpy change (ΔH) indicates that the processes are endothermic; however, the 3-$CuCl_2$ association is mainly affected by temperature and the entropy change (ΔS), with a low contribution of the enthalpy (ΔH) as previously reported [52].

Moreover, fluorescence recovery was investigated through the addition of EDTA (see Fig. 8). The **3-CuCl$_2$** interaction was not reversible with the addition of EDTA. In these tests, the same incubation time was used as in the previous experiments (time = 3 min). However, this phenomenon is not strange since in other investigations, this tendency has also been shown [53].

Table 1
Thermodynamic parameters of the interaction of compound **3** and $CuCl_2$.

	ΔG (kJ/mol)	ΔH (kJ/mol)	ΔS (J/mol)
298 K	−5.39	41.3	156
308 K	−4.18		147

Finally, to rule out that the quenching of the fluorescence of compound**3** is due to the water added in the test, the $CuCl_2$ solution was replaced by distilled water. Our results show that there is no significant change in the fluorescence intensity when adding water (see Supplementary Material Figure S6).

3.3. Theoretical approach

Using the Gaussian 09 program, the minimal energy structures of compound **3** and the **3-CuCl$_2$** complex were optimized using DFT-B3LYP-LanL2DZ in the gas phase. The electrostatic potential map of compound **3** (see Fig. 9A) shows an area with a negative charge density (red colour) where it can generate the interaction between **3** and $CuCl_2$ through the electron lone pairs of nitrogen. Therefore, the formation of complex **3-CuCl$_2$**is plausible through the nitrogen atom.

Likewise, the HOMO and LUMO for compound **3** and the **3-CuCl$_2$** complex (see Fig. 9B and C and Fig. 9E and F) were calculated because they have important contributions to electronic photo-excitation transitions [54]. Comparing the molecular orbitals of compound **3** with those of the **3-CuCl$_2$** complex, it can be seen that the HOMO and LUMO are mainly located on the α,β-unsaturated imine (see Fig. 9B and C). However, when plotting the HOMO and LUMO of the **3-CuCl$_2$** complex, a displacement can be seen. The HOMO is between the phenylhydrazone fragment and the chloride substituents of $CuCl_2$, while the LUMO is centred on the metal (see Fig. 9E and F).

Comparing the energies associated with the HOMO-LUMO transition (assigned by us to the $\pi \rightarrow \pi^*$ transition of the chromophore), it can be seen that for compound **3,** the energy associated with this transition corresponds to 3.70 eV ($\lambda = 335$ nm), which is consistent with the maximum absorption wavelength measured ($\lambda = 359$ nm). In the **3-CuCl$_2$** complex, the energy of the same transition is 1.97 eV ($\lambda = 629$ nm). However, this transition is not consistent with the $CuCl_2 \rightarrow 3$ charge transfer signal ($\lambda = 459$ nm, see Fig. 2). In this sense, it has been reported that HOMO-1→LUMO transitions may be associated with

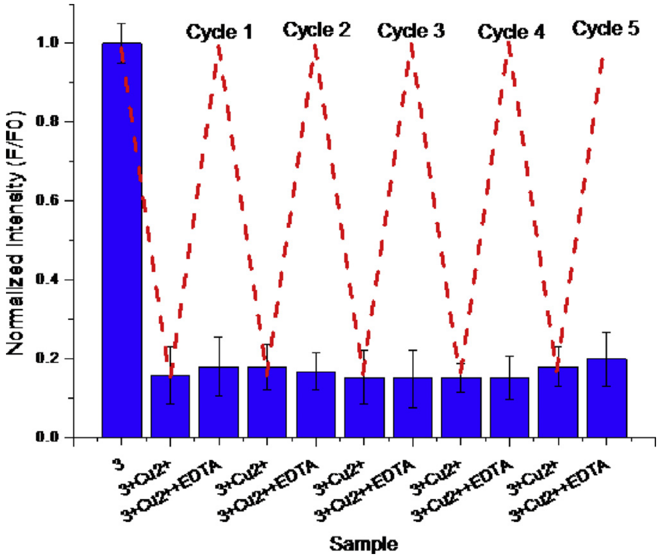

Fig. 8. Fluorescence recovery from the **3-CuCl$_2$** interaction using EDTA. $C_3 = 20$ μM, solvent = MeCN, $\lambda_{ex} = 394$ nm, $\lambda_{em} = 476$ nm, T° = 298 K, $t_{incubation} = 3$ min, n = 3.

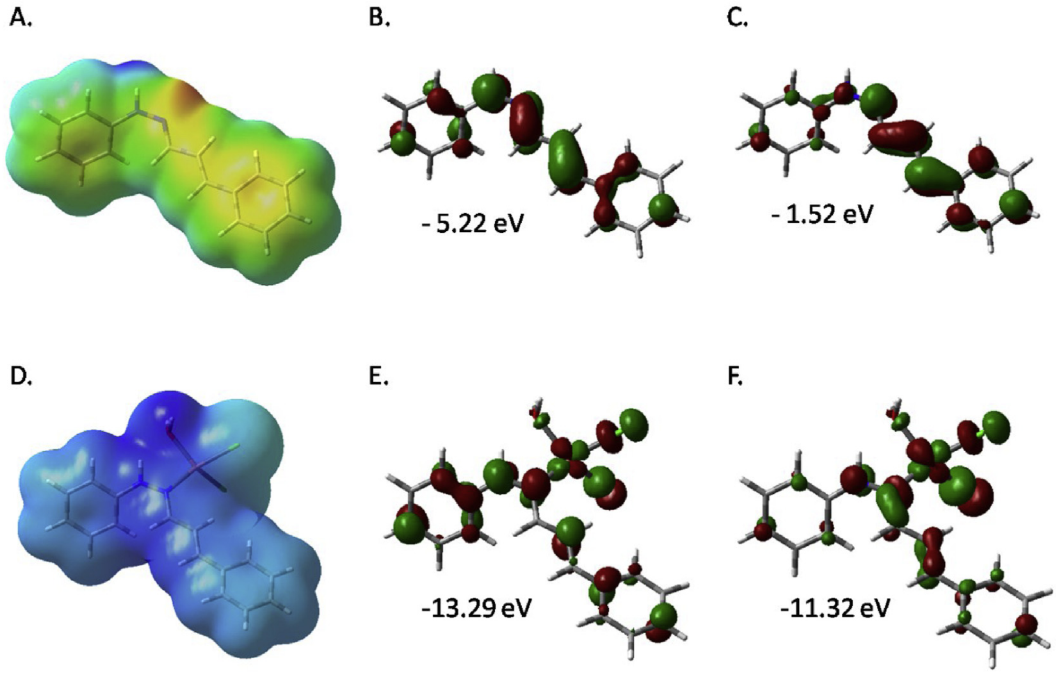

Fig. 9. A. Map of the electrostatic potential of compound **3**. B. HOMO of compound **3**. C. LUMO of compound **3**. D. Map of the electrostatic potential of compound **3-CuCl$_2$**. E. HOMO of compound **3-CuCl$_2$**. F. LUMO of compound **3-CuCl$_2$**. Isovalue = 0.04; density = 0.0004.

photophysical phenomena [54,55]. In effect, this calculated electronic transition is nearest to the absorption band shown in the UV–Vis spectra, λ = 459 nm (see Supplementary Material Figure S7).

In addition, through quantitative structure-property relationship (QSPr) techniques, various correlations were evaluated between the different physicochemical properties of the inorganic salts tested (independent variables) and the normalized variation of the fluorescence (dependent variable). The correlation obtained is shown in Eq. (11).

$$F/F_0 = 0.96 + 0.240\,\mathbf{LUMO} + 0.130\omega - 0.003\omega^2$$
$$n = 18; r = 0.904; r^2 = 0.817; SD = 0.099; F = 20.9; q^2 = 0.777 \qquad (\text{Eq. }11)$$

Eq. (11) indicates that the fluorescence quenching is related to the energy of the LUMO and to the global electrophilic index (ω) of the different inorganic salts, which are descriptors related to the ability to accept electrons and their stabilization [56,57]. This result confirms that the interaction between **3-CuCl$_2$** corresponds to an interaction of molecular orbitals forming the corresponding complex (see Supplementary Material Figure S8).

With this information obtained from the computational approach, a fluorescence mechanism based on internal charge transfer is proposed (see Scheme 2). The fluorescence of compound **3**is decreased due to the coordination of the pairs of non-bonding electrons of the imine nitrogen by charge transfer from the metal to compound **3**.

3.4. Quantitation assays of Cu^{2+} in water samples

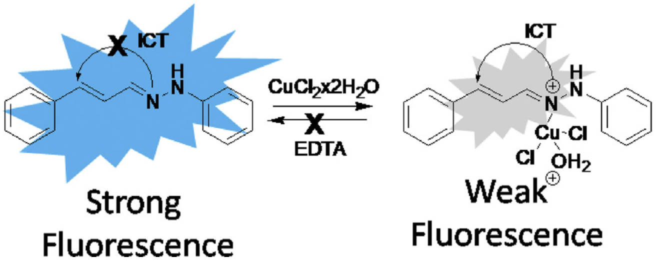

Scheme 2. Proposed fluorescence mechanism for compound **3** and its interaction with CuCl$_2$.

The potential application of compound **3** as a copper sensor in different water samples was tested. Samples of deionized, potable and well water (Carpintero and Pitama) were used under the same conditions applied in this investigation (C_3 = 20 μM, solvent = MeCN, incubation time = 3 min, temperature = 298 K). The results are summarized in Table 2.

The measurements of CuCl$_2$ in the different water samples showed that the recovery of CuCl$_2$ is similar in the well water from Carpintero and Pitama (111.8% and 99.3%, respectively) at concentrations greater than 40 μM. However, for the detection and quantification of CuCl$_2$ at concentrations that are close to or under current U.S.-EPA regulations for drinking water, the analyte recovery rate decreases significantly (66.4% in drinking water and 72.5% in deionized water).

4. Conclusions

Cinnamaldehyde phenylhydrazone (**3**) was synthesized in high

Table 2
Determination of Cu^{2+} using compound **3** in different water samples.

Sample	Cu^{2+}added (μM)	Cu^{2+}found (μM)[a]	Recovery (%)
Drinking water	14	9.3 ± 0.35	66.4
Carpintero's well water	44	49.2 ± 8.5	111.8
Pitama's well water	72	71.5 ± 3.2	99.3
Deionized water	28	20.3 ± 0.01	72.5

[a] Experiment carried out three times.

yield (81% yield). Its photophysical properties (UV–Vis and fluorescence) were evaluated in the absence and presence of various metals, and it was found that $CuCl_2$ causes selective quenching of the fluorescence intensity and decay of the quantum yield in a thermodynamically spontaneous process ($\Delta G < 0$).

Using quantitative structure-activity (QSAR) techniques, it was determined that the fluorescence intensity is affected by the transfer of electrons from HOMO of compound **3** to the LUMO of $CuCl_2$, quenching the fluorescence in an internal charge transfer (ICT) process.

The quantification and detection of $CuCl_2$ was performed using four different water samples, and it was found that at concentrations greater than 40 μM, all dissolved $CuCl_2$ was recovered. However, at concentrations below 20 μM, the recovery rate decreased to 66.4%. Despite these results, the information obtained in this investigation can be applied to the design of new chemosensors based on compound **3**.

Declaration of competing interest

We declare that we have no conflicts of interest to this work. We declare that we do not have any commercial or associative interest that represents a conflict of interest in connection with the work submitted.

Funding

This work was supported by the ANID [Fondecyt Postdoctoral grant 3180408, Fondecyt 1190752]; and VRIEA-PUCV [37.0/2017].

Declaration of competing interest

The authors declare that they have no known competing financial interests or personal relationships that could have appeared to influence the work reported in this paper.

CRediT authorship contribution statement

Marco Mellado: Conceptualization, Methodology, Software, Investigation, Formal analysis, Funding acquisition, Resources, Writing - review & editing. **Rafaela Sariego-Kluge:** Methodology, Formal analysis. **César González:** Methodology, Investigation. **Katy Díaz:** Methodology, Investigation. **Luis F. Aguilar:** Supervision, Writing - review & editing. **Manuel A. Bravo:** Resources, Writing - review & editing.

Acknowledgements

The authors thank to Agencia Nacional de Investigación y Desarrollo (ANID) and Vicerrectoría de Investigación y Estudios Avanzados of Pontificia Universidad Católica de Valparaíso (VRIEA-PUCV).

Appendix A. Supplementary data

Supplementary data to this article can be found online at https://dx.doi.org/10.1016/j.molstruc.2020.128430

References

[1] N. Giuseppone, J.L. Schmitt, E. Schwartz, J.M. Lehn, Scandium(III) catalysis of transimination reactions. Independent and constitutionally coupled reversible processes, J. Am. Chem. Soc. 127 (15) (2005) 5528–5539.

[2] B. Kocyigit-Kaymakcioglu, E.E. Oruc-Emre, S. Unsalan, S. Rollas, Antituberculosis activity of hydrazones derived from 4-fluorobenzoic acid hydrazide, Med. Chem. Res. 18 (4) (2009) 277–286.

[3] A.B.A. El-Gazzar, H.N. Hafez, G.A.M. Nawwar, New acyclic nucleosides analogues as potential analgesic, anti-inflammatory, anti-oxidant and antimicrobial derived from pyrimido[4,5-b]quinolines, Eur. J. Med. Chem. 44 (4) (2009) 1427–1436.

[4] B.F. Abdel-Wahab, G.E.A. Awad, F.A. Badria, Synthesis, antimicrobial, antioxidant, anti-hemolytic and cytotoxic evaluation of new imidazole-based heterocycles, Eur. J. Med. Chem. 46 (5) (2011) 1505–1511.

[5] A.E. Kummerle, M. Schmitt, S.V.S. Cardozo, C. Lugnier, P. Villa, A.B. Lopes, N.C. Romeiro, H. Justiniano, M.A. Martins, C.A.M. Fraga, J.J. Bourguignon, E.J. Barreiro, Design, synthesis, and pharmacological evaluation of N-Acylhydrazones and novel conformationally constrained compounds as selective and potent orally active phosphodiesterase-4 inhibitors, J. Med. Chem. 55 (17) (2012) 7525–7545.

[6] S. Bala, G. Uppal, S. Kamboj, V. Saini, D.N. Prasad, Design, characterization, computational studies, and pharmacological evaluation of substituted-N '-[(1E) substituted-phenylmethylidene]benzohydrazide analogs, Med. Chem. Res. 22 (6) (2013) 2755–2767.

[7] D.D. Gaikwad, A.D. Chapolikar, C.G. Devkate, K.D. Warad, A.P. Tayade, R.P. Pawar, A.J. Domb, Synthesis of indazole motifs and their medicinal importance: an overview, Eur. J. Med. Chem. 90 (2015) 707–731.

[8] S. Emami, S. Dadashpour, Current developments of coumarin-based anticancer agents in medicinal chemistry, Eur. J. Med. Chem. 102 (2015) 611–630.

[9] G. Roman, Mannich bases in medicinal chemistry and drug design, Eur. J. Med. Chem. 89 (2015) 743–816.

[10] U. Abu Mohsen, B. Kocyigit-Kaymakcioglu, E.E. Oruc-Emre, Z.A. Kaplancikli, S. Rollas, Studies on hydrazide-hydrazones derivatives as acetylcholinesterase inhibitors, Clin Exp Health Sci 5 (1) (2015) 10–14.

[11] K. Kucukoglu, M. Gul, M. Atalay, E. Mete, C. Kazaz, O. Hanninen, H.I. Gul, Synthesis of some Mannich bases with dimethylamine and their hydrazones and evaluation of their cytotoxicity against Jurkat cells, Arzneim. Forsch. 61 (6) (2011) 366–371.

[12] K. Kucukoglu, H.I. Gul, R. Cetin-Atalay, Y. Baratli, A.L. Charles, M. Sukuroglu, M. Gul, B. Geny, Synthesis of new N,N '-bis[1-aryl-3-(piperidine-1-yl)propylidene]hydrazine dihydrochlorides and evaluation of their cytotoxicity against human hepatoma and breast cancer cells, J. Enzym. Inhib. Med. Chem. 29 (3) (2014) 420–426.

[13] K. Kucukoglu, H.I. Gul, M. Gul, R. Cetin-Atalay, Y. Baratli, B. Geny, Cytotoxicity of hydrazones of morpholine bearing mannich bases towards Huh7 and T47D cell lines and their effects on mitochondrial respiration, Lett. Drug Des. Discov. 13 (8) (2016) 734–741.

[14] V. Jyothi, N. Babu, P.K. Reddy, T. Ashwini, Synthesis, characterization and evaluation of anti-tubercular, anti-inflammatory and anti-microbial activities of newer hydrazones, Inven. Rapid MedChem 4 (2014) 1–6, 2014.

[15] E.I. Khizhan, A.I. Khizhan, G.A. Tikhonova, V.Y. Maslova, Antioxidant activity of arylhydrazones in sunflower oil oxidation, Russ. J. Appl. Chem. 85 (3) (2012) 460–464.

[16] T.B. Chaston, R.N. Watts, J. Yuan, D.R. Richardson, Potent antitumor activity of novel iron chelators derived from di-2-pyridylketone isonicotinoyl hydrazone involves fenton-derived free radical generation, Clin. Canc. Res. 10 (21) (2004) 7365–7374.

[17] X.F. Bao, Y. Xue, C. Xia, Y. Lu, N.J. Yang, Y. Zhao, Synthesis and Assessment of novel anti-chlamydial benzylidene Acylhydrazides derivatives, Lett. Drug Des. Discov. 15 (1) (2018) 31–36.

[18] K. Hruskova, E. Potuckova, T. Hergeselova, L. Liptakova, P. Haskova, P. Mingas, P. Kovarikova, T. Simunek, K. Vavrova, Aroylhydrazone iron chelators: tuning antioxidant and antiproliferative properties by hydrazide modifications, Eur. J. Med. Chem. 120 (2016) 97–110.

[19] C.R. Li, Z.C. Liao, J.C. Qin, B.D. Wang, Z.Y. Yang, Study on 2-Acetylpyrazine (pyridine-2 '-acetyl) hydrazone as a fluorescent sensor for Al3+, J. Lumin. 168 (2015) 330–333.

[20] X. Su, I. Aprahamian, Hydrazone-based switches, metallo-assemblies and sensors, Chem. Soc. Rev. 43 (6) (2014) 1963–1981.

[21] S.J. Jiang, J.B. Qiu, Y.X. Chen, H.Y. Guo, F.F. Yang, Luminescent columnar liquid crystals based on AIE tetraphenylethylene with hydrazone groups bearing multiple alkyl chains, Dyes Pigments 159 (2018) 533–541.

[22] T. Aysha, M. El-Sedik, S. Abd El Megied, H. Ibrahim, Y. Youssef, R. Hrdina, Synthesis, spectral study and application of solid state fluorescent reactive disperse dyes and their antibacterial activity, Arab J Chem 12 (2) (2019) 225–235.

[23] D. Debnath, S. Roy, B.H. Li, C.H. Lin, T.K. Misra, Synthesis, structure and study of azo-hydrazone tautomeric equilibrium of 1,3-dimethyl-5-(arylazo)-6-amino-uracil derivatives, Spectrochim. Acta 140 (2015) 185–197.

[24] B. Samanta, J. Chakraborty, S. Shit, S.R. Batten, P. Jensen, J.D. Masuda, S. Mitra, Synthesis, characterisation and crystal structures of a few coordination complexes of nickel(II), cobalt(III) and zinc(II) with N '-[(2-pyridyl)methylene] salicyloylhydrazone Schiff base, Inorg. Chim. Acta. 360 (7) (2007) 2471–2484.

[25] H. Jansova, J. Kubes, P. Reimerova, P. Sterbova-Kovarikova, J. Roh, T. Simunek, 2,6-Dihydroxybenzaldehyde analogues of the iron chelator salicylaldehyde isonicotinoyl hydrazone: increased hydrolytic stability and cytoprotective activity against oxidative stress, Chem. Res. Toxicol. 31 (11) (2018) 1151–1163.

[26] G.M. Abu El-Reash, O.A. El-Gammal, A.H. Radwan, Molecular structure and biological studies on Cr(III), Mn(II) and Fe(III) complexes of heterocyclic carbohydrazone ligand, Spectrochim. Acta 121 (2014) 259–267.

[27] N.H. Al-Shaalan, Synthesis, characterization and biological activities of Cu(II),

Co(II), Mn(II), Fe(II), and UO2(VI) complexes with a new Schiff base hydrazone: O-Hydroxyacetophenone-7-chloro-4-quinoline hydrazone, Molecules 16 (10) (2011) 8629–8645.
[28] X.Y. Zhu, Y.A. Duan, P. Li, H.M. Fan, T.Y. Han, X.N. Huang, A highly selective and instantaneously responsive Schiff base fluorescent sensor for the "turn-off" detection of iron(iii), iron(ii), and copper(ii) ions, Anal Methods-Uk 11 (5) (2019) 642–647.
[29] C. Rj, Zinc, in: F.L. Ziegler EE (Ed.), Knowledge in Nutrition, ILSI Press, Washington, DC, 1996, pp. 293–306.
[30] P.C. Dhar, A. Pal, P. Mohanty, B. Bag, Colorimetric detection of Cu(II) ion with a 1,3-bis-azachalcone derivative, Sensor. Actuator. B Chem. 219 (2015) 308–314.
[31] C.R. Chen, G.W. Men, W.H. Bu, C.S. Liang, H.C. Sun, S.M. Jiang, A colorimetric and fluorescent probe for multiple transition metal ions (Cu2+, Zn2+ and Ni2+): fast response and high selectivity, Sensor. Actuator. B Chem. 220 (2015) 463–471.
[32] S. Mukherjee, S. Betal, Sensing phenomena, extraction and recovery of Cu2+ followed by smart phone application using a luminescent pyrene based chemosensor, J. Lumin. 204 (2018) 145–153.
[33] J.R. Lakowicz, Principles of Fluorescence Spectroscopy, second ed., Kluwer Academic/Plenum Publishers, New York, London, Moscow, Dordrecht, 1999.
[34] K. Nawara, J. Waluk, Improved method of fluorescence quantum yield determination, Anal. Chem. 89 (17) (2017) 8650–8655.
[35] M. Thompson, S.L.R. Ellison, R. Wood, Harmonized guidelines for single-laboratory validation of methods of analysis, Pure Appl. Chem. 74 (5) (2002) 835–855.
[36] M.J. Frisch, G.W. Trucks, H.B. Schlegel, G.E. Scuseria, M.A. Robb, J.R. Cheeseman, G. Scalmani, V. Barone, G.A. Petersson, H. Nakatsuji, X. Li, M. Caricato, A. Marenich, J. Bloino, B.G. Janesko, R. Gomperts, B. Mennucci, H.P. Hratchian, J.V. Ortiz, A.F. Izmaylov, J.L. Sonnenberg, D. Williams-Young, F. Ding, F. Lipparini, F. Egidi, J. Goings, B. Peng, A. Petrone, T. Henderson, D. Ranasinghe, V.G. Zakrzewski, J. Gao, N. Rega, G. Zheng, W. Liang, M. Hada, M. Ehara, K. Toyota, R. Fukuda, J. Hasegawa, M. Ishida, T. Nakajima, Y. Honda, O. Kitao, H. Nakai, T. Vreven, K. Throssell, J. Montgomery, J A, J.E. Peralta, F. Ogliaro, M. Bearpark, J.J. Heyd, E. Brothers, K.N. Kudin, V.N. Staroverov, T. Keith, R. Kobayashi, J. Normand, K. Raghavachari, A. Rendell, J.C. Burant, S.S. Iyengar, J. Tomasi, M. Cossi, J.M. Millam, M. Klene, C. Adamo, R. Cammi, J.W. Ochterski, R.L. Martin, K. Morokuma, O. Farkas, J.B. Foresman, D.J. Fox, Gaussian 09 Revision A.02, Gaussian Inc., Wallingford CT, 2016.
[37] M. Mellado, A. Madrid, M. Reyna, C. Weinstein-Oppenheimer, J. Mella, C.O. Salas, E. Sanchez, M. Cuellar, Synthesis of chalcones with antiproliferative activity on the SH-SY5Y neuroblastoma cell line: quantitative Structure-Activity Relationship Models, Med. Chem. Res. 27 (11–12) (2018) 2414–2425.
[38] M. Mellado, A. Madrid, U. Martinez, J. Mella, C.O. Salas, M. Cuellar, Hansch's analysis application to chalcone synthesis by Claisen-Schmidt reaction based in DFT methodology, Chem. Pap. 72 (3) (2018) 703–709.
[39] A. Golbraikh, A. Tropsha, Beware of q(2)!, J. Mol. Graph. Model. 20 (4) (2002) 269–276.
[40] K.G. Rajam, M.P. Kumar, K.J. Kiran, Shivaraj, mixed ligand complexes derived from semicarbazone Schiff base and heterocyclic ligands: structure and antimicrobial activity, Russ. J. Gen. Chem. 88 (5) (2018) 1000–1008.
[41] M.P. Kumar, N. Vamsikrishna, G. Ramesh, N.J.P. Subhashini, J.B. Nanubolu, Shivaraj, Cu(II) complexes with 4-amino-3,5-dimethyl isoxazole and substituted aromatic aldehyde Schiff bases: synthesis, crystal structure, antimicrobial activity, DNA binding and cleavage studies, J. Coord. Chem. 70 (8) (2017) 1368–1388.
[42] S. Biju, S.S. Kumar, V. Sadasivan, Synthesis, spectral and single crystal X-ray characterization of 5-(2-(2,3-dimethyl-5-oxo-1-phenyl-2,5-dihydro-1H-pyrazol-4-yl)hydrazono)pyrimidine-2,4,6(1H,3H,5H)-trione and its copper(II) complexes, Polyhedron 144 (2018) 210–218.
[43] K. Ponnuvel, M. Kumar, V. Padmini, A new quinoline-based chemosensor for Zn2+ ions and their application in living cell imaging, Sensor. Actuator. B Chem. 227 (2016) 242–247.
[44] A.K. Mahapatra, G. Hazra, N.K. Das, S. Goswami, A highly selective triphenylamine-based indolylmethane derivatives as colorimetric and turn-off fluorimetric sensor toward Cu^{2+} detection by deprotonation of secondary amines, Sensor. Actuator. B Chem. 156 (1) (2011) 456–462.
[45] C.Q. Jiang, B. Tang, R.Y. Wang, J.C. Yen, Spectrofluorimetric determination of trace amounts of aluminium with 5-bromo-salicylaldehyde salicyloylhydrazone, Talanta 44 (2) (1997) 197–202.
[46] X. Zheng, K.H. Lee, H. Liu, S.Y. Park, S.S. Yoon, J.Y. Lee, Y.G. Kim, A bis(pyridine-2-ylmethyl)amine-based selective and sensitive colorimetric and fluorescent chemosensor for Cu2+, Sensor. Actuator. B Chem. 222 (2016) 28–34.
[47] G.Y. Lan, C.C. Huang, H.T. Chang, Silver nanoclusters as fluorescent probes for selective and sensitive detection of copper ions, Chem Commun 46 (8) (2010) 1257–1259.
[48] H.A. Benesi, J.H. Hildebrand, A spectrophotometric investigation of the interaction of iodine with aromatic hydrocarbons, J. Am. Chem. Soc. 71 (8) (1949) 2703–2707.
[49] H. Liu, F.X. Li, Y. Pi, D.J. Wang, Y.J. Hu, J. Zheng, Fluorescence quenching study of 2,6-bis(5-(4-methylphenyl)-1-H-pyrazol-3-yl)pyridine with metal ions, Spectrochim. Acta 145 (2015) 588–593.
[50] C. Wang, Q.H. Wu, C.R. Li, Z. Wang, J.J. Ma, X.H. Zang, N.X. Qin, Interaction of tetrandrine with human serum albumin: a fluorescence quenching study, Anal. Sci. 23 (4) (2007) 429–433.
[51] M. Calvin, N.C. Melchior, Stability of chelate compounds. IV. Effect of the metal ion, J. Am. Chem. Soc. 70 (10) (1948) 3270–3273.
[52] K.S. Siddiqi, S. Bano, A. Mohd, A.A.P. Khan, Binding interaction of captopril with metal ions: a fluorescence quenching study, Chin. J. Chem. 27 (9) (2009) 1755–1761.
[53] L.L. Li, H. Li, G. Liu, S.Z. Pu, A colorimetric and fluorescent chemosensor for selective detection of Cu2+ based on a new diarylethene with a benzophenone hydrazone unit, Luminescence 32 (8) (2017) 1473–1481.
[54] A. Frazer, A.R. Morales, A.W. Woodward, P. Tongwa, T. Timofeeva, K.D. Belfield, Luminescent fluorene-based bis-pyrazolyl Aniline ligand for Aluminum detection, J. Fluoresc. 24 (1) (2014) 239–250.
[55] K. Gayathri, K. Velmurugan, R. Nandhakumar, M. Malathi, S. Mathusalini, P.S. Mohan, R. Shankar, New pyrazolo-quinoline scaffold as a reversible colorimetric fluorescent probe for selective detection of Zn2+ ions and its imaging in live cells, J. Photochem. Photobiol., A 341 (2017) 136–145.
[56] J.E. López, A.E. Ensuncho, J.R. Robles, Global and local reactivity descriptors for the design of new anticancer drugs based on cis-platinum(II), Quim. Nova 36 (9) (2013) 1308–1317.
[57] R.G. Pearson, The principle of maximum hardness, Accounts Chem. Res. 26 (5) (1993) 250–255.